buildings

MDPI

Article

Enhancing the Strength and Durability of Cement Mortar: Synergetic Effects of Shell Powder, Calcium Formate and Basalt Fibers

Wei Shi [1,*], Zhongping Tang [1], Yiming Jin [2], Shixiang Yi [1], Lili Huang [1], Shuang Lu [3,*] and Wenjing Sun [4]

[1] Institute of Structural Material Failure and Strengthening Technology, Ningbo Polytechnic University, Ningbo 315000, China; 2022005@nbpt.edu.cn (Z.T.); 1001554@nbpt.edu.cn (S.Y.); 0809102@nbpt.edu.cn (L.H.)
[2] School of Civil and Environmental Engineering, Ningbo University, Ningbo 315000, China; t1143193109@163.com
[3] School of Physics and Materials Science, Changji University, Changji 831100, China
[4] State Key Laboratory of Intelligent Deep Metal Mining and Equipment, Northeastern University, Shenyang 110819, China
* Correspondence: alice7882@126.com (W.S.); lus@hit.edu.cn (S.L.)

Abstract

This study focuses on the core issue of sustainably utilizing shells to enhance the performance of cement mortar. The influence of shell powder on the slump flow, setting time, mechanical strengths, drying shrinkage rate and carbonation depth of cement mortar is investigated. The flexural and compressive strengths of cement mortar incorporating calcium formate after 12 h, 3-day and 28-day curing periods are examined. The effect of basalt fibers on the attenuation of cement mortar's mechanical properties (flexural and compressive strengths) after NaCl freeze–thaw cycles is also studied. Scanning electron microscopy-energy dispersive spectroscopy (SEM-EDS) is employed to elucidate the underlying mechanisms. Results show that the slump flow, setting time and mechanical strengths have cubic function relationships with the shell powder's mass ratio, while the drying shrinkage rate and carbonation depth follow quadratic function changes. Cement mortar with 15% shell powder by mass of the total binder materials demonstrates the highest slump flow and mechanical strengths. At this shell powder mass ratio, cement mortar shows the lowest drying shrinkage rate and carbonation depth. Calcium formate positively influences the 12-h mechanical strengths. After 3 days of curing, the mechanical strengths of cement mortar with 0.3% calcium formate are the highest. The calcium carbonate powder reduces the drying shrinkage rate of mortar and increases the content of Ca and C elements. The mass ratio of calcium formate exhibits a negative correlation with the cement mortar's mechanical strengths after being cured for 28 days. The addition of basalt fibers enhances resistance to chloride salt freeze–thaw and dry-wet alternations erosion performance. These findings will provide a sustainable and effective strategy for utilizing agricultural by-products in concrete structures.

Keywords: shell powder; slump flow; setting time; mechanical strengths; calcium formate; basalt fibers; chloride salt

Check for updates

Academic Editor: Salvatore Verre

Received: 20 November 2025
Revised: 20 December 2025
Accepted: 23 December 2025
Published: 25 December 2025

Copyright: © 2025 by the authors. Licensee MDPI, Basel, Switzerland. This article is an open access article distributed under the terms and conditions of the Creative Commons Attribution (CC BY) license.

1. Introduction

Shells are calcified structures formed through secretions from specialized glandular cells in mollusks, serving as a protective covering for their soft bodies. As natural and

renewable resources, shells primarily consist of angular columnar calcium carbonate crystals and organic substances [1,2]. In recent years, the disposal of large quantities of shell waste from aquaculture and seafood industries has become a significant environmental burden [3]. Current disposal methods include processing shells into animal feed, food additives, medicinal herbs and adsorbents, representing viable approaches for waste treatment and pollution mitigation [4]. These applications remain limited in their capacity to handle the vast quantities of shell waste generated annually [5]. Consequently, developing more effective and scalable disposal methods represents an urgent necessity.

The production of cement-based materials heavily relies on non-renewable natural resources. To reduce this dependence and promote a circular economy, shell powder, as a typical agricultural waste product, has the potential to be used as an auxiliary cementitious material or filler [6]. Therefore, the research of systematically evaluating the impact of shell powder on the performance of cement mortar can provide a scientific basis for its resource utilization, thereby reducing the consumption of primary minerals in the construction industry.

Chen et al. [7] have reported that shell powder can effectively enhance the freeze resistance of cement concrete. Jeong et al. [8] have found that 10% shell powder by mass of binder materials can increase the cement concrete's slump by up to 2.6%. Moreover, the shell powder has been proven to reduce cement concrete's total pore volume by 25%. Naqi et al. [9] have found 6% calcined oyster shell powder increases the 3-day compressive strength by 60%, maintains comparable 28-day strength and slightly improves long-term performance (7% at 91 days), attributing its role in promoting hydration and refining pore structure. However, prior research indicates that excessive shell powder application may cause calcium ion enrichment and inhibit hydration reactions, leading to reduced mid-term strength [10]. Jing et al. [11] report that the shell powder can increase the mechanical strengths of potassium magnesium phosphate cement-based material when its mass ratio is lower than 30%. However, the shell powder with a mass ratio of higher than 30% exhibits detrimental effects on the potassium magnesium phosphate cement-based material's mechanical strengths [12]. Although several studies have investigated shell powder concrete, limited research has addressed the corrosion behavior of shell powder cement-based materials in chloride environments [13–15]. Furthermore, no precedent exists for using early-strength agents in shell powder cement-based materials to develop rapid-repair materials. Calcium formate, a common early-strength agent for silicate cement-based materials, has been shown to significantly enhance compressive strengths [16–18]. As pointed out in a previous study, the calcium formate can increase the compressive strengths of silicate cement concrete by rates of up to 16.6% [19]. Nevertheless, the influence of calcium formate on the properties of shell powder cementitious materials has received limited research attention.

So far, several kinds of fibers (steel fibers, polypropylene fibers and carbon fibers) are employed for the reinforcement of cement concrete [20]. The steel fibers significantly enhance the mechanical strengths and durability of cement-based materials. However, steel fibers are susceptible to corrosion when the reinforced materials are exposed to chloride-rich environments [21,22]. Other fibers, such as polypropylene fibers and carbon fibers, demonstrate limited effectiveness in enhancing the mechanical and durable properties of cement-based materials [23]. The basalt fibers were used as reinforced fibers in cement-based materials, due to their natural, pollution-free, strong compatibility with concrete, and easy dispersion in cement-based materials [24].

This study systematically investigates the fluidity, setting time and mechanical strengths of shell powder cement mortar at 3-day and 28-day curing ages. It further examines the influence of calcium formate on the mechanical strengths at 12 h, 3-day and

28-day curing periods and evaluates the effect of varying volume ratios of basalt fibers on mechanical performance. The drying shrinkage rate and carbonation depth of cement mortar with 5~40% shell powder are measured. The mechanisms underlying these property variations are elucidated through scanning electron microscopy–energy dispersive spectroscopy (SEM-EDS) analysis.

2. Materials and Methods

2.1. Raw Materials

The shell powder and ultra-fine silica powder used in this study were supplied by Shanghai Shengtongwei Trading Co., Ltd., Shanghai, China. The shell powder showed a specific surface area and density of 10,500 m^2/kg and 2.6 g/cm^3. Meanwhile, the specific surface area and density of this ultra-fine silica powder were 14,800 m^2/kg and 2.2 g/cm^3. The ordinary Portland cement (P·O) used in this study was supplied by Zhejiang Huier Cement Co., Ltd., Quzhou, China, showing a compressive strength grade of 42.5 MPa. This cement exhibited an initial setting time of 113 min, a final setting time of 215 min, a density of 3.04 g/cm^3 and a specific surface area of 321 m^2/kg. Quartz sand with particle sizes of (0.68–1.21) mm, (0.33–0.61) mm and (0.14–0.31) mm, sourced from the mineral processing facility of Henan Lianxin Activated Carbon Co., Ltd., Gongyi, China, was utilized as aggregate in this research. To regulate the flowability of fresh cement mortar, a pale yellow polycarboxylic water-reducing agent with a 41.2% water-reducing capacity was employed. Solid content and density of concrete water-reducing agent were 23.1% and 1.07 g/cm^3, respectively. The standards for ultra-fine silica powder, ordinary Portland cement and concrete water-reducing agent were in accordance with GB/T 27690-2023, GB 175-2023, GB/T 14684-2022 and GB 8076-2008 [25–28].

The physical properties, chemical composition and particle size distribution of the powder materials were presented in Tables 1–3, respectively. The particle size distribution of the raw materials is presented in Figure 1.

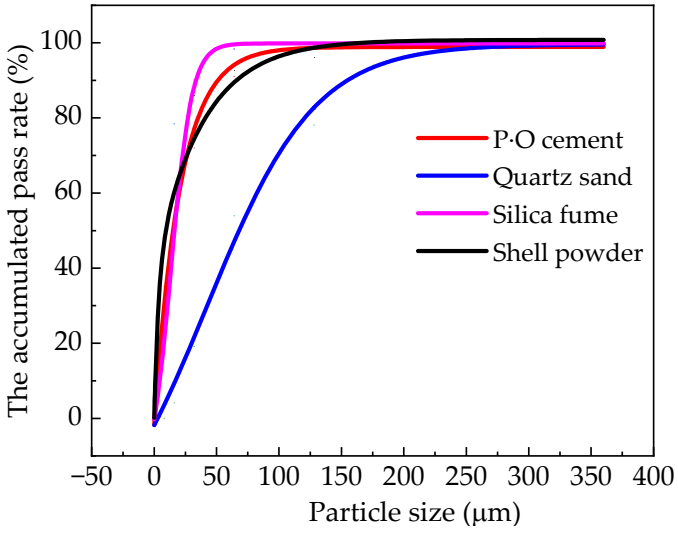


Figure 1. Particle size distribution of the raw materials.

Table 1. Physical and basic properties of the raw materials.

Material	Specific Surface Area (m^2/kg)	Density (g/cm^3)	Compressive Strength Grade (MPa)	Initial Setting Time (min)	Final Setting Time (min)
Shell powder	10,500	2.6	-	-	-
P·O cement	321	3.04	42.5	113	215
Silica fume	14,800	2.2	-	-	-
Quartz sand	-	-	2.65	-	-
Water-reducing agent	-	-	1.07	-	-

Table 2. The particle size distribution of the cementitious materials (%).

Types	Particle Size/μm						
	0.3	**0.6**	**1**	**4**	**8**	**64**	**360**
Shell powder	0.15	7.2	23.8	72.1	83.2	97.3	100
P·O cement	0.09	0.31	2.59	14.96	28.44	92.66	100
Silica fume	31.01	57.97	81.66	100	100	100	100
Quartz sand	0	0	0	0	0.04	20.81	100

Table 3. The chemical composition of cementitious materials (%).

Types	SiO_2	Al_2O_3	Fe_xO_y	MgO	CaO	SO_3	K_2O	Na_2O	Ca_2CO_3	P_2O_5	Loss on Ignition
Shell powder	0.49	0.53	-	0.32	-	0.21	0.52	0.54	95.03	0.32	2.02
P·O cement	20.61	5.51	3.77	1.78	62.45	2.76	-	-	-	-	3.12
Silica fume	90.76	0.22	0.62	0.21	0.43	0.21	7.54	-	-	-	-
Quartz sand	99.73	-	0.27	-	-	-	-	-	-	-	-

2.2. Samples Manufacturing

The mixing proportions of the cement mortar specimens are detailed in Table 4. Fresh cement mortar was prepared using a UJZ mixer supplied by Beijing Luda Instrument Manufacturing Factory (Beijing, China). The water-to-binder (w/b) ratio was maintained at 0.40 for the mixtures. All powder materials (the specified dosages of shell powder and calcium formate, according to Table 3) were first introduced into a UJZ-15 mixer and agitated at 60 r/min for 1 min. For mixtures containing basalt fibers, the fibers were added at the beginning of the first minute to ensure uniform dispersion. Subsequently, the uniformly blended solution containing the water-reducing agent and water was introduced and mixed at a mixing speed of 80 r/min for an additional 210 s. This mixing procedure was conducted in accordance with the Chinese standard JGJ/T 70-2009 [29]. Following the mixing process, the fresh cement mortar was immediately used for slump flow measurement according to the Chinese standard GB/T 2419-2005 [30]. After evaluating the fluidity, specimens measuring 40 × 40 × 160 mm^3 were cast according to GB/T 17671-2021 [31] for determining flexural strengths, compressive strengths and drying shrinkage rate.

Table 4. Shell powder cement mortar mixing proportions (kg/m^3).

Water	P·O Cement	Shell Powder	Silica Fume	Quartz Sand	Water-Reducer	Shell Powder/Total Binder Materials
370.4	740.7	0	185.2	977.9	3.7	0%
370.4	703.66	37.04	185.2	977.9	3.7	5%
370.4	666.63	74.07	185.2	977.9	3.7	10%
370.4	629.69	111.11	185.2	977.9	3.7	15%
370.4	592.56	148.14	185.2	977.9	3.7	20%
370.4	555.52	185.18	185.2	977.9	3.7	25%
370.4	518.49	222.21	185.2	977.9	3.7	30%
370.4	481.45	259.25	185.2	977.9	3.7	35%
370.4	444.42	296.28	185.2	977.9	3.7	40%

2.3. Measuring Methods

2.3.1. The Slump Flow and the Setting Time

The NLD-3 jumping-table apparatus produced by Beijing Zhongke Lujian Instrument Equipment Co., Ltd., Beijing, China, was employed to measure the slump flow of fresh cement mortar. The fresh cement mortar was added to the round platform with a height of 60 mm, upper inner diameter of 70 mm and lower inner diameter of 100 mm in two layers. After the addition, the mold was lifted vertically. Then, the mortar needed to be vibrated 25 times at a frequency of 1 Hz with the NLD-3 jumping table. Finally, the maximum diameter and its perpendicular diameter of the spread mortar were measured. The average value of the two diameters was taken as the slump flow. Slump flow determination followed the Chinese standard GB/T2419-2005 [30]. The setting time of cement mortar was determined using the ZKS-100 mortar setting time tester manufactured by Wuxi Jianyi Instrument Machinery Co., Ltd., Wuxi, China, equipped with a test needle having a cross-sectional area of 30 mm^2. The instrument applied pressures of 0.3 MPa and 0.7 MPa to determine the initial and final setting times, respectively. The detailed measurement procedures of slump flow and setting time were conducted in accordance with the Chinese standard JGJ/T 70-2009 [29].

2.3.2. The Mechanical Strengths and Dry Shrinkage Rate

Specimens for mechanical strength testing were cured under standard conditions (a temperature of 20 ± 2 °C and a relative humidity of 98.4%). The detailed process was described as follows. A three-point bending test was conducted using a carbon material bending apparatus (Shanghai Hualong Testing Instrument Co., Ltd., Shanghai, China). The specimen was placed on two supporting rollers with a span of 100 mm. A concentrated load was applied at the mid-span through a loading roller at a constant loading rate of 0.05 kN/s until failure. Immediately after the flexural test, the two broken halves of each specimen were used for the compressive strength test. Each half was placed centrally in a compression testing fixture (Shanghai Hualong Testing Instrument Co., Ltd.) with a 40 × 40 mm^2 loading area. A uniaxial compressive load was applied at a constant rate of 2.4 kN/s until failure. The mechanical performance evaluation of cement mortar was selected based on both the early performance and the long-term design standards: the 3-day compressive strength was used to reflect the early performance related to the construction progress, and the 28-day compressive strength was taken as the benchmark indicator for long-term structural design. This selection method complied with the requirements of the standard test specification (GB/T 17671-2021 [31]).

The drying shrinkage rate was measured according to the following procedure. Firstly, the specimens with a size of 40 × 40 × 160 mm^3 were installed on the drying shrinkage

test rack, and the drying shrinkage value was collected by the Mitutoyo original Japanese Sanfeng digital altimeter gauge measuring instrument digital micrometer, provided by New Sanfeng Precision Measuring Tool Enterprise Store, Shanghai, China. The dry shrinkage rate was conducted in accordance with the Chinese standard JC/T 603-2004 [32].

2.3.3. Chloride Salt Erosion

In the NaCl erosion experiments, all specimens were immersed in the 3% NaCl solution for 4 days after being cured in a standard environment for 24 days. Following immersion, the specimens were placed in airtight freeze–thaw containers (stainless-steel) filled with 3% NaCl solution, which were then loaded into a TRDF-2 fully automatic rapid freeze–thaw test chamber (Tianjin Huida Test Instrument Co., Ltd., Tianjin, China). The freeze–thaw cycling process was subsequently initiated. Each rapid freeze–thaw cycle was completed within 2 h to 4 h, with temperatures ranging from −20 °C to 20 °C. All processes were carried out in accordance with the standard GB/T 50082-2024 [33].

In the NaCl dry-wet alternation experiment, the specimens were immersed in NaCl solution following the same procedure as used for the NaCl freeze–thaw cycles. Following the soaking process, the specimens were relocated to an LSB concrete corrosion resistance dry-wet cycle tester (manufactured by Suzhou Donghua Experimental Instrument Co., Ltd., Suzhou, China). Each dry–wet cycle consisted of immersing the specimens in NaCl solution for 8 h, followed by wiping their surfaces dry with a cloth. Thereafter, the specimens were subjected to drying at 80 °C for 36 h, followed by a 2 h cooling period. The mechanical strengths were measured per 100 NaCl dry–wet alternations. Detailed procedures followed the aforementioned methodology.

2.3.4. Microscopic Experimental Process

To achieve the microscopic structure analysis at the nanoscale and the precise correspondence of micro-area chemical composition, further screening and processing were carried out from the previously prepared particles to obtain ellipsoidal samples with a maximum diameter of less than 0.5 mm. These samples were cleaned and thoroughly dried, and then underwent gold spraying treatment under vacuum conditions to form a uniform conductive film, ensuring stable imaging under high-energy electron beams.

Subsequently, the sample was placed in the sample chamber of the SEM4000Pro field emission scanning electron microscope (produced by Beijing Zhongke Keqi Co., Ltd., Beijing, China). This equipment was operated under typical working parameters (such as an acceleration voltage set at 15 kV, a beam current of approximately 1 nA, and a working distance maintained at around 10 mm) to balance high-resolution imaging and effective X-ray excitation. Under these conditions, a combined analysis of scanning electron microscopy–energy dispersive spectroscopy (SEM-EDS) was conducted. The specimens preparation and experimental process are presented in Figure 2.

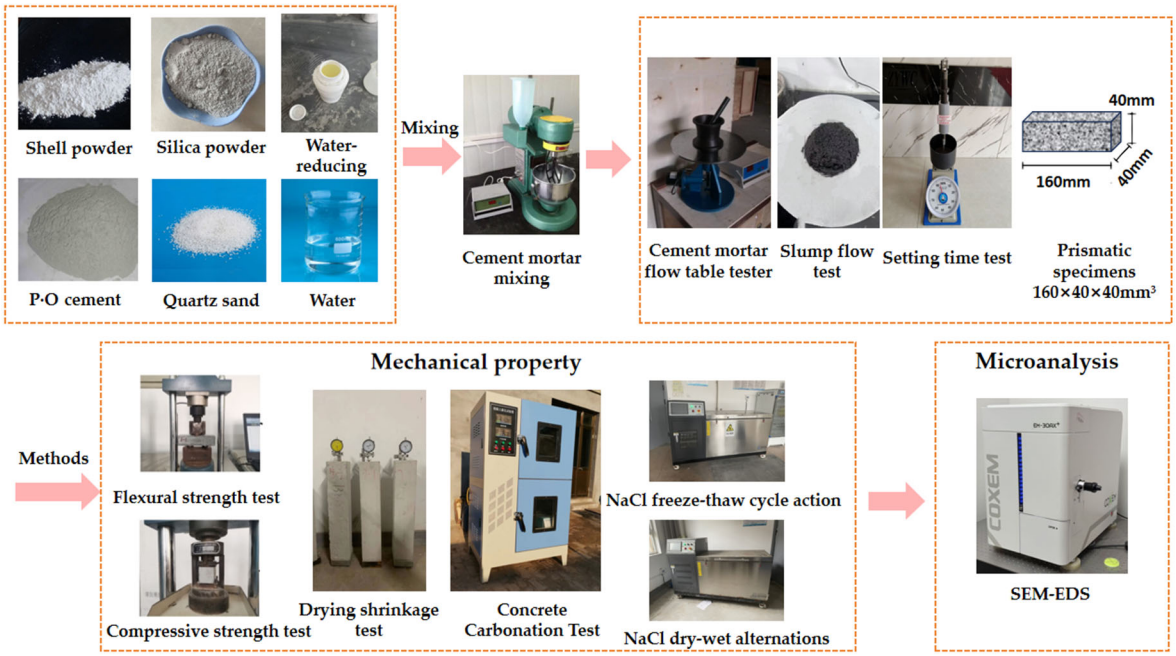


Figure 2. Specimen preparation and experimental process.

3. Results and Discussion

3.1. Fluidity and Setting Time

Figure 3 presents the slump flow of fresh cement mortar with varying shell powder contents. As shown, the slump flow of cement mortar varies in the form of cubic functions with the mass ratio of shell powder. The cement mortar with 15% shell powder achieves the maximum slump flow. The added shell powder can increase the slump flow by up to 7.7%. The error bars, representing the standard deviation derived from sextuplicate measurements, do not exceed 8% of the corresponding mean values, indicating good repeatability of the experimental data. This behavior can be attributed to the spherical morphology of shell powder particles, which enhances slump flow at incorporation rates of 0–15% [16]. However, when the mass ratio of shell powder increases from 15% to 40%, the slump flow decreases by 2.8~17.6%. This is ascribed to the fact that the shell powder possesses a higher specific surface area than the cement [34]. Hence, the shell powder reduces the fresh cement mortar's fluidity.

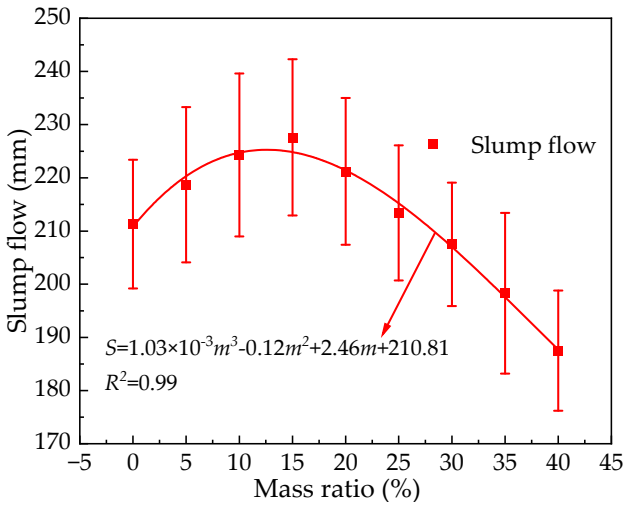


Figure 3. The slump flow of fresh cement mortar with shell powder.

The initial and final setting times of cement mortar with varying mass ratios of shell powder are displayed in Figure 4. As depicted in Figure 4, the initial and final setting time of cement mortar grow as cubic functions. The initial setting time ranges from 48.8% to 58.2% of the final setting time. The error bars remain within 3.9~7.3% of the actual values of the initial and final setting time. The addition of shell powder by a mass ratio of 5~40% can increase the initial and final setting time by 12.5~103.8% and 15.0~78.0%. This retardation effect is attributed to the lower hydration activity of shell powder compared to cement [35].

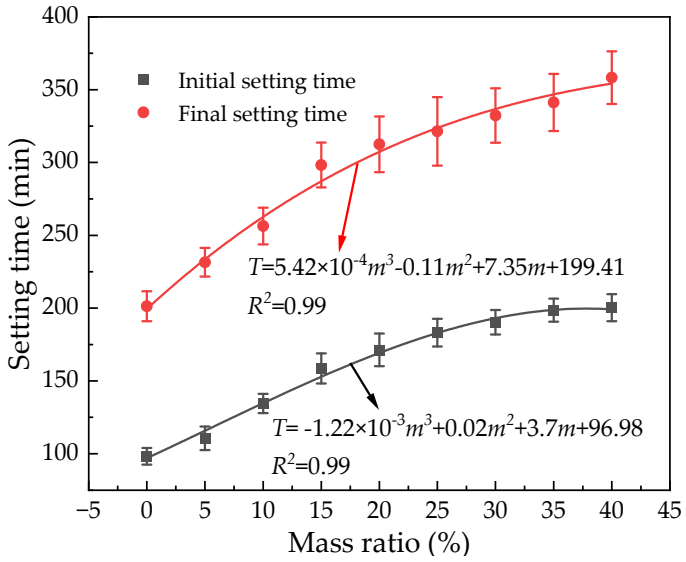
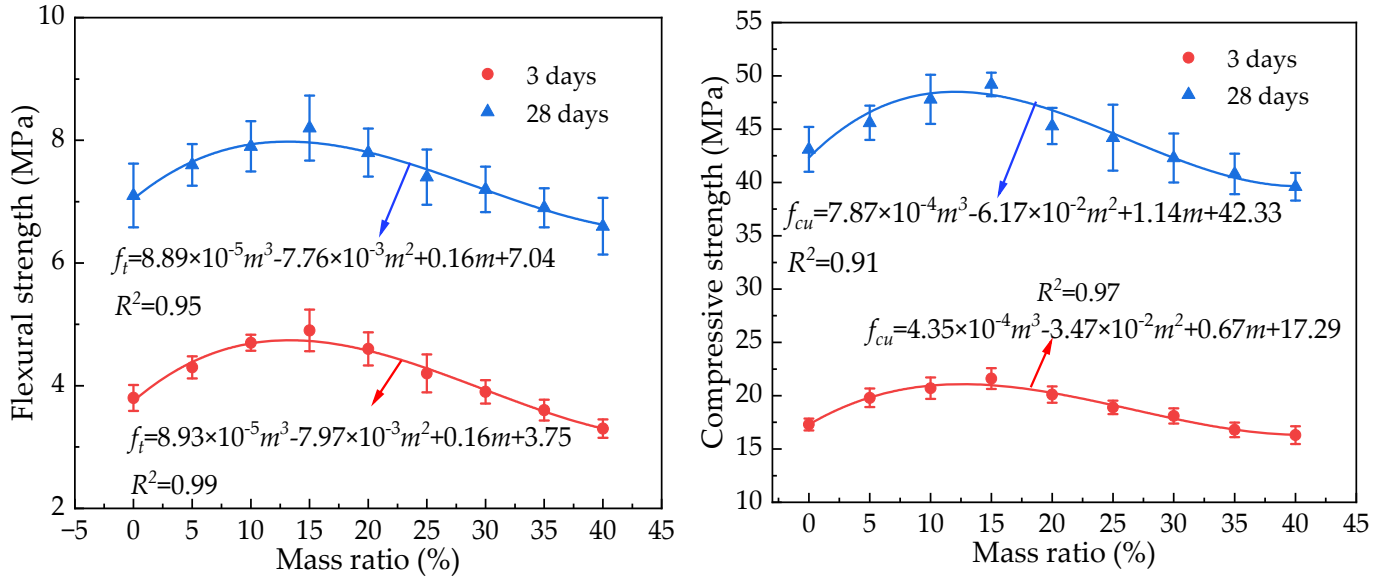


Figure 4. The setting time of cement mortar with shell powder.

3.2. The Mechanical Strengths

Figure 5 displays the flexural and compressive strengths of cement mortar with different shell powder mass ratios. As shown, the mechanical strengths of cement mortar vary in the form of cubic functions with the mass ratio of shell powder. Cement mortar with 15% shell powder demonstrates the maximum mechanical strength. The 3-day flexural strengths and 3-day compressive strengths of cement mortar are 50~59.8% and 40.1~44.4% of the 28-day flexural strengths and 28-day compressive strengths. The error bars of the mechanical strengths are 2.8~7.4% of the real mechanical strengths, which ensures the precision of the experiment. The added shell powder at a mass ratio of 15% enhances the 3-day flexural strength, 3-day compressive strength, 28-day flexural strength and 28-day compressive strength by up to 32.7%, 24.5%, 19.5% and 19.8%. This improvement arises because the shell powder optimizes the particle size distribution of cementitious materials, thereby increasing the mechanical strengths of shell powder cement mortar [36]. Moreover, the shell powder interacts with calcium sulfate hemihydrate, forming more compact hydration products [37]. Therefore, the mechanical strengths are decreased when the mass ratio of shell powder is higher than 15%. Excessive addition of shell powder causes an increase in calcium ion concentration, which inhibits the hydration of cement [38]. When calcium ions are excessively enriched in a local or overall solution, it significantly increases the ionic strength of the solution, through the like-ion effect, inhibiting the further dissolution of calcium ions in cement minerals (such as C_3S and C_3A), thereby fundamentally slowing down the supply of hydration reactants [39].



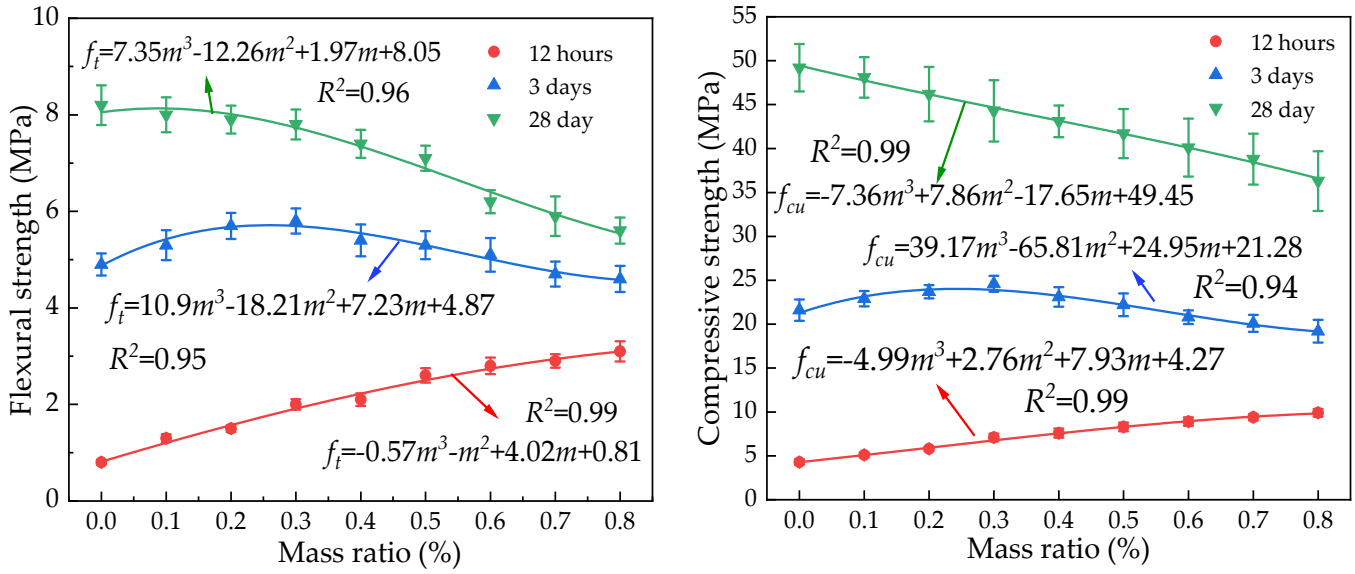
(**a**) Flexural strength (**b**) Compressive strength

Figure 5. The mechanical strengths of cement mortar with shell powder.

Figure 6 presents the mechanical strengths of cement mortar with different calcium formate mass ratios after 12 h, 3-day and 28-day curing periods. As found in Figure 6, the mechanical strengths vary in the form of cubic functions with the mass ratio of the calcium formate. When the specimens are cured for 12 h, the mechanical strengths increase with the addition of calcium formate. The calcium formate with the mass ratio of 0~0.8% can increase the 12 h-flexural strength and 12 h-compressive strengths by 62.5~287.5% and 18.6~130.2%. This improvement is attributed to the accelerating effect of calcium formate on Portland cement setting, which enhances early-age strength development [40]. Specimens with 0.3% calcium formate show the highest mechanical strengths when the specimens are cured for 3 days. At this curing age, the calcium formate can increase the flexural and compressive strengths by up to 18.4% and 13.9%. Meanwhile, the calcium formate at a mass ratio of 0.8% can decrease the flexural and compressive strengths by rates of up to 6.1% and 11.1%. The added calcium formate decreases the flexural and compressive strengths by rates of up to 46.4% and 35.5%. This can be explained by the fact that the calcium formate can promote the setting of cement, leading to an increase in early hydration heat and cracks, which in turn results in a decrease in its later strength [41]. The error bars are all less than 9.4% of the actual mechanical strengths, confirming experimental accuracy.

3.3. The Drying Shrinkage

Figure 7 presents the drying shrinkage rate of shell powder cement mortar with different shell powder mass ratios. As shown, the dry shrinkage rate of cement mortar decreases in the form of a quadratic function. In total, 5~40% of shell powder by mass ratio of the total binder materials can decrease the dry shrinkage rate by rates of 1.65~10.99% and 4.49~12.46%. This can be attributed to the fact that the shell powder can reduce the hydration degree of cement, thus reducing the dry shrinkage rate of the cement mortar [42]. The dry shrinkage rate increases by 54.2~58.8% when the curing age increases from 3 days to 28 days. This increase occurs because specimens cured for 28 days attain a higher hydration degree compared to those cured for 3 days, resulting in greater drying shrinkage. The addition of shell powder can reduce the drying shrinkage rate of cement mortar by up to 12.5%.



(**a**) Flexural strength (**b**) Compressive strength

Figure 6. The mechanical strengths of shell powder cement mortar with calcium formate.

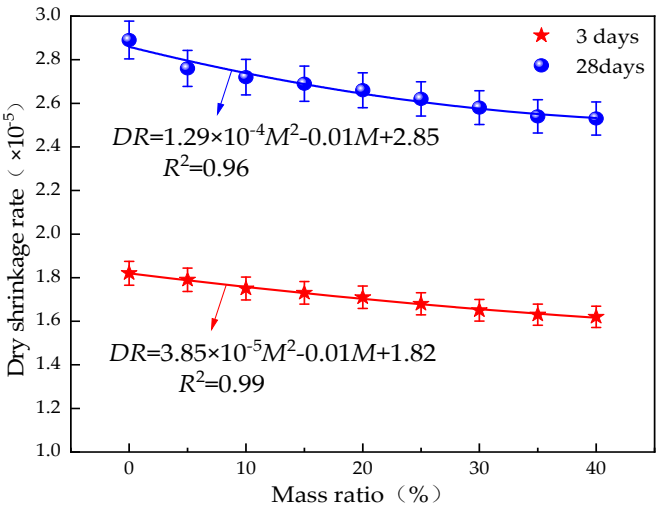


Figure 7. The dry shrinkage rate of shell powder cement mortar with different mass ratios of shell powder.

3.4. The Carbonation Depth

The carbonation depth of cement mortar with different mass ratios of shell powder is shown in Figure 8. As found in this part, the carbonation depth decreases in the form of quadratic functions when the mass ratio increases from 0% to 15%. Due to the improved grading and hydration degree, the mortar becomes more compact [43]. Therefore, the permeability of CO_2 into cement mortar is decreased, leading to a decrease in the carbonation depth. Meanwhile, when the mass ratio increases from 15% to 40%, the carbonation depth increases. This is because the excessive mass ratio of shell powder exhibits a negative effect on the hydration degree, resulting in a reduction in hydration products' compactness and increasing the carbonation depth [44]. The addition of shell powder can reduce the drying shrinkage rate of cement mortar by up of rates 24.6%.

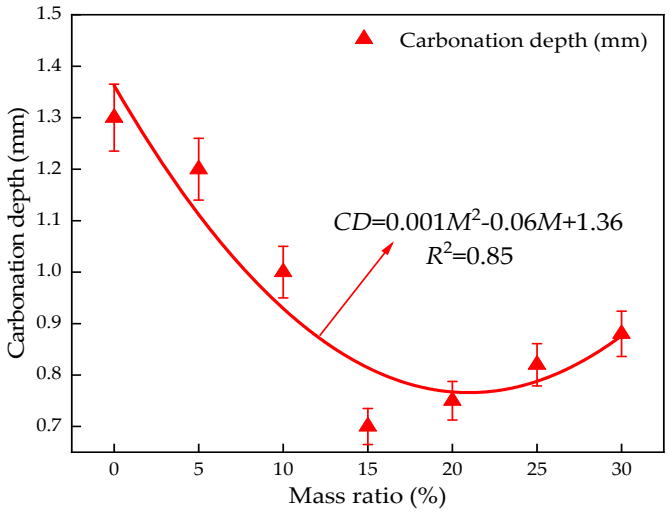


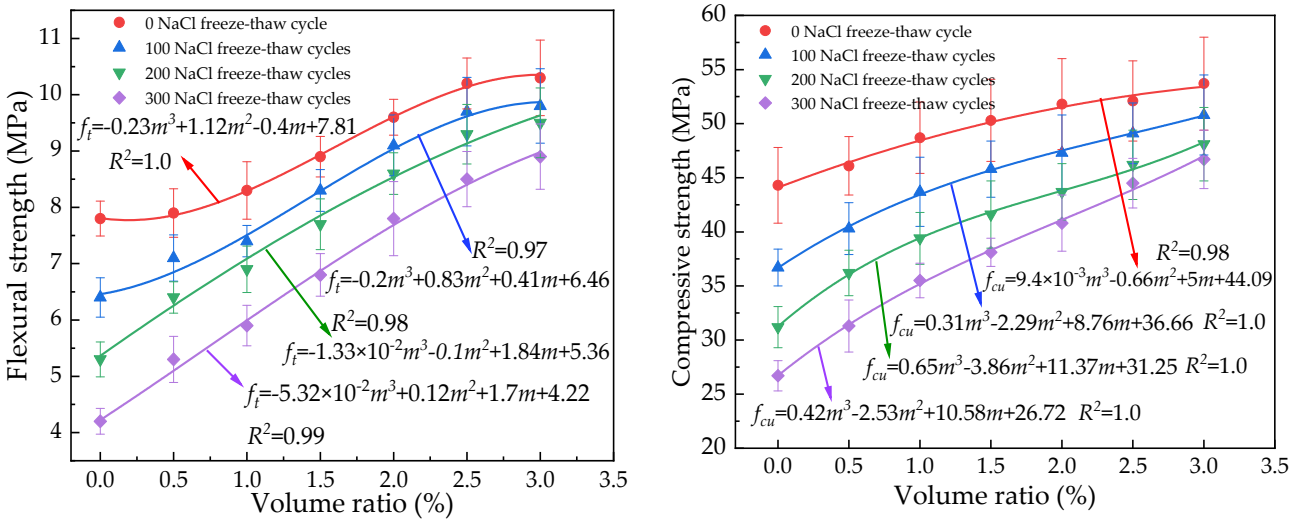
Figure 8. The carbonation depth of cement mortar with different mass ratios of shell powder.

3.5. Mechanical Strengths After NaCl Erosion

Figure 9 presents the flexural and compressive strengths of cement mortar after exposure to different numbers of NaCl freeze–thaw cycles. As shown in Figure 9, the mechanical strengths increase in the form of cubic functions with the volume ratios of basalt fibers. With 0, 100, 200 and 300 freeze–thaw cycles, the flexural strengths increase by 1.28~32.05%, 10.93~53.12%, 20.75~79.24% and 26.19~111.90%, respectively, at basalt fiber volume ratios of 0.5~3%. Under the same conditions, the compressive strengths improve by 4.06~21.22%, 9.81~38.42%, 16.03~54.17% and 17.23~74.91%. This enhancement is attributed to the bridging effect of basalt fibers in the cement mortar, which delays the degradation of mechanical properties under freeze–thaw cycles [45]. Conversely, the flexural strengths decrease by 4.85–17.95%, 7.77–32.05% and 13.59–46.15% after 100, 200 and 300 freeze–thaw cycles, while the compressive strengths decline by 5.40–17.16%, 10.42–29.57% and 13.04–39.73%, respectively. These reductions result from the expansion of internal cracks caused by crystallization pressure and frost heave stress during freeze–thaw cycles [34]. The error bars remain within 3.33–8.46% of the actual mechanical strengths, confirming the reliability of the experimental data. The exceptional resistance of the mortar to 300 NaCl freeze–thaw cycles is attributed to the synergistic interaction between shell powder and basalt fibers. The incorporation of shell powder refines the pore structure through micro-filling and nucleation effects, significantly reducing the content of freezable water and the permeability of the matrix, thereby mitigating the driving forces of frost damage and salt crystallization [46]. Simultaneously, the well-dispersed basalt fibers form a three-dimensional network that effectively bridges micro-cracks induced by cyclic stresses, preventing their propagation into critical macro-cracks [47].

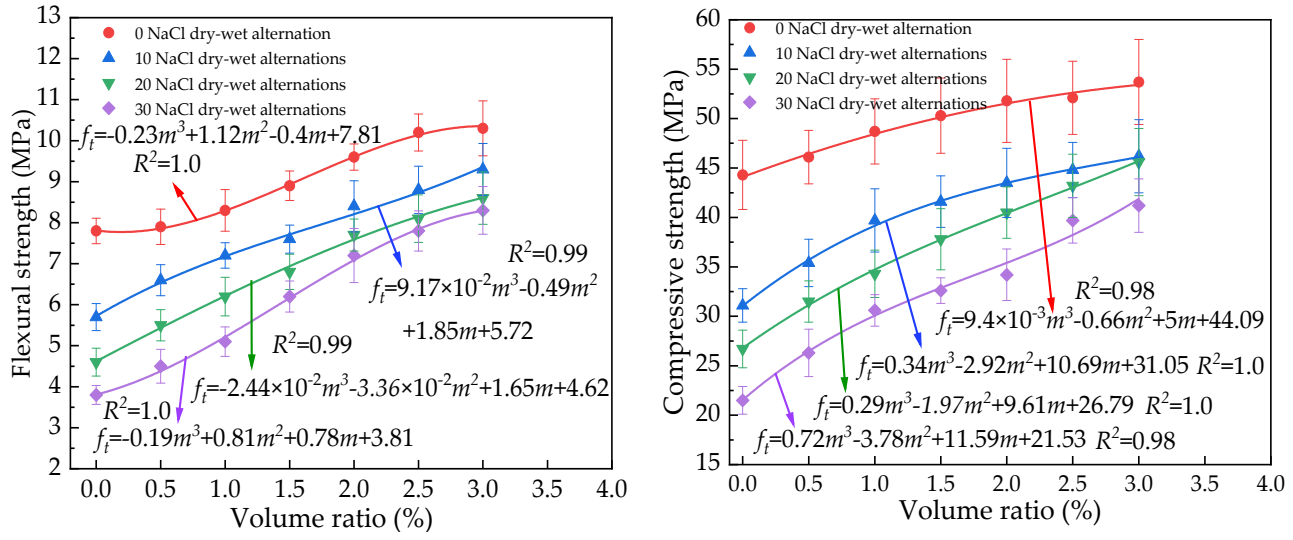
Figure 10 displays the mechanical strengths of cement mortar with different basalt fiber volume ratios after exposure to varying numbers of NaCl dry-wet alternations. As shown, the mechanical strengths of cement mortar vary in the form of cubic functions with the basalt fibers' volume ratio. The incorporation of 0.5–3% basalt fibers enhances the flexural strengths by 1.28–32.05%, 15.79–63.16%, 19.57–86.96% and 18.42–118.42% after 0, 10, 20 and 30 dry-wet alternations, respectively. Correspondingly, the compressive strengths increase by 4.06–21.21%, 13.83–48.55%, 17.98–70.79% and 22.33–91.63% under the same conditions. This improvement stems from the crack-bridging capability of basalt fibers, which restricts crack propagation in the cement matrix under dry–wet cycling. However, the flexural strengths decreased by rates of 9.71~26.92%, 16.50~41.03% and 19.42~51.28% after 10, 20 and 30 NaCl dry-wet alternations. Meanwhile, the corresponding compressive

strengths are decreased by rates of 13.97~29.80%, 15.08~39.73% and 23.28~51.47%, when the number of NaCl dry–wet alternations is 10, 20 and 30. These reductions are attributed to the cyclic crystallization stress developed during the dry–wet alternation process [48]. The error bars are 3.33~9.17% of the real values of mechanical strengths, indicating the experimental accuracy.



(**a**) Flexural strength (**b**) Compressive strength

Figure 9. The mechanical strengths of shell powder cement mortar with basalt fibers after suffering different numbers of NaCl freeze–thaw cycles.

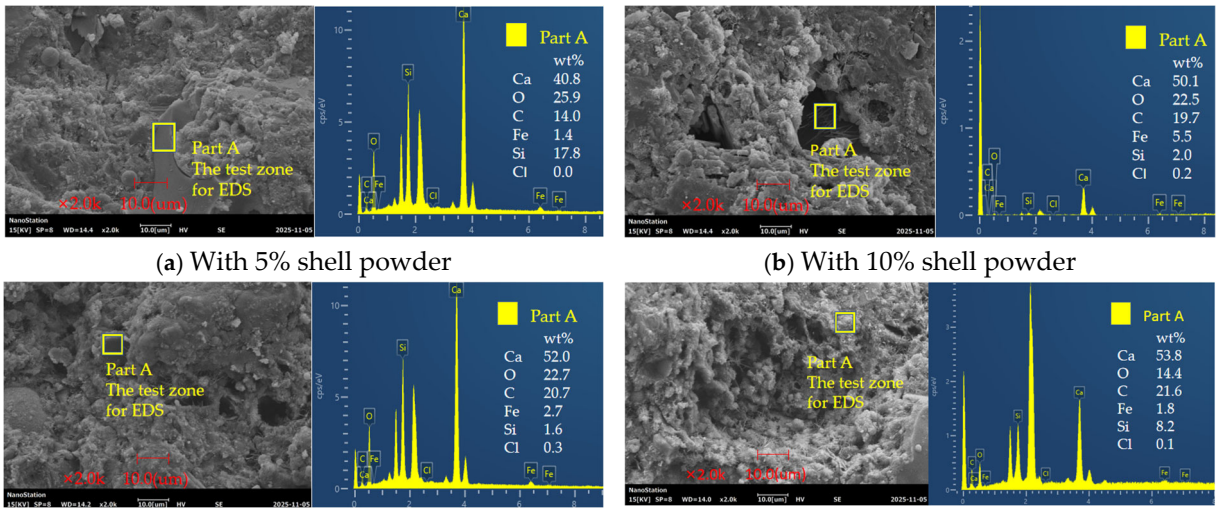


(**a**) Flexural strength (**b**) Compressive strength

Figure 10. The mechanical strengths of shell powder cement mortar with basalt fibers after suffering different numbers of NaCl dry-wet alternations.

3.6. Microscopic Results

Figure 11 presents the scanning electron microscopy–energy dispersive spectroscopy (SEM-EDS) results of cement mortar containing varying dosages of shell powder, cured under standard conditions for 28 days.



(**a**) With 5% shell powder (**b**) With 10% shell powder

(**c**) With 15% shell powder (**d**) With 20% shell powder

Figure 11. SEM-EDS of cement mortar with different dosages of shell powder.

The EDS spectra consistently detect the presence of calcium (Ca), oxygen (O), carbon (C), iron (Fe), silicon (Si) and chlorine (Cl) across all samples. This trend is a direct consequence of the primary chemical composition of shell powder (calcium carbonate ($CaCO_3$)) [49]. The incorporation of shell powder, therefore, acts as an external source of both calcium and carbon ions, enriching the cement matrix with these elements. Furthermore, the detection of trace chlorine (Cl) can be attributed to the natural history of the shell feedstock. Shells harvested from marine environments undergo prolonged immersion in seawater, leading to the adsorption and retention of chloride ions within their porous structure [50]. This explains the persistent, albeit weak, Cl signal observed in the EDS analysis.

The corresponding SEM micrographs in Figure 11 reveal distinct morphological features of the hydration products. A mixture of needle-like (likely ettringite) and flocculent (typical of calcium silicate hydrate, C-S-H) phases is identified, which aligns with the common microstructure of hydrated Portland cement systems [51]. More critically, the microstructural density shows a clear dependency on the shell powder dosage. At lower incorporation levels (5% to 15%), the shell powder particles act as effective micro-fillers and nucleation sites, promoting the formation of a more abundant and densely packed C-S-H gel, as seen in the increasingly consolidated matrix from Figure 11a–c. This refinement effect is well-documented for fine $CaCO_3$ fillers, which accelerate cement hydration and refine pore structure [52]. However, beyond an optimal threshold (15% in this study), excessive shell powder appears to dilute the cementitious components and may disrupt the cohesive formation of hydration products. As observed in Figure 11d, the microstructure at 20% shell powder content appears slightly more porous and less uniform compared to the 15% specimen. The summary of microscopic results is presented in Table 5.

Table 5. Summary of microscopic results.

Analysis Dimension	Observation Results and Conclusions
Major element	Ca, O, C, Fe, Si and Cl
Key element changes	The addition of shell powder increases the content of calcium and carbon.
Changing reason	The main component of shell powder is calcium carbonate. It introduces additional calcium and carbon into the cement matrix.
Source of chlorine element	The shells were soaked in seawater for a long time before use, resulting in residual chloride ions in the powder.
Microstructure	Observed needle-like and flocculent hydrolysis products.
Structural compactness change	When the content of shell powder is between 5% and 15%, the density of the hydration product increases; when it is between 15% and 20%, the density decreases.
Optimal performance point	The specimens with a 15% admixture content had the highest density of hydration products, and the mechanical properties reached the optimal level at this admixture content.

4. Conclusions

This study investigates the properties and chloride salt erosion resistance of shell powder cement mortar. The main findings are summarized as follows.

(1) The slump flow and the setting time of fresh shell powder cement mortar vary in the form of cubic functions with the mass ratio of shell powder. When the shell powder is within the range of 5% to 40%, the fluidity increases, with the maximum increase being 7.7%, but the setting time has been significantly prolonged.

(2) The correlation between the shell powder cement mortar's mechanical strengths and the mass ratio of shell powder coincides with cubic functions. Cement mortar containing 15% shell powder shows the highest mechanical strengths. At this dosage, the 3-day flexural strengths, 3-day compressive strengths, 28-day flexural strengths, and 28-day compressive strengths increase by up to 28.9%, 24.9%, 15.5% and 14.2%, respectively. However, excessive addition will reduce the strength of the cement due to the inhibition of its hydration process. The relationships between the drying shrinkage and carbonation depth conform to quadratic functions. Shell powder helps to reduce the drying shrinkage rate and carbonation depth of the mortar. Cement mortar with 15% shell powder exhibits the lowest drying shrinkage and carbonation depth.

(3) As an early-strength agent, calcium formate can significantly enhance the ultra-early (12 h) strength of mortar (with the compressive strength increasing by up to approximately 130%), but it has a negative impact on the long-term strength at 28 days. But the added basalt fibers enhance both the mechanical strengths and chloride salt erosion resistance of the calcium formate cement mortar.

(4) Microscopic analysis indicates that the incorporation of calcium formate increases the calcium and carbon content in cement mortar. At a 15% concentration, the hydration product has the densest structure, which is consistent with the optimal performance of macroscopic mechanical properties and durability. In conclusion, by blending 15% of shell powder with an appropriate amount of basalt fiber, the mechanical properties of cement mortar can be enhanced and the durability against chloride salt erosion can be improved. When using cement mortar containing 15% shell powder, calcium formate can meet the early strength requirements for rapid repair. This research provides a reliable theoretical basis and practical ratio guidance for the large-scale and high-value resource utilization of shell waste. The research results can be directly applied to the production of building materials in coastal areas, the repair of engineering structures in corrosive environments, and the development of high-performance ecological mortars required for green buildings, demonstrating significant environmental benefits and engineering application prospects.

Author Contributions: Conceptualization, S.L. and W.S. (Wei Shi); methodology, S.L.; validation, S.L. and W.S. (Wei Shi); formal analysis, W.S. (Wei Shi) and Y.J.; investigation, Z.T., S.Y. and S.L.; resources, W.S. (Wei Shi); data curation, Z.T. and Y.J.; writing—original draft preparation, W.S. (Wei Shi) and S.Y.; writing—review and editing, S.Y., L.H., Z.T. and S.L.; visualization, Y.J.; supervision, W.S. (Wei Shi); project administration, W.S. (Wenjing Sun) and S.L.; funding acquisition, L.H. and S.L. All authors have read and agreed to the published version of the manuscript.

Funding: This work is sponsored by the Key technologies for preparing a new type of shell-based vegetation concrete for environmental restoration in southern forest areas [No. 2024NFLY02].

Data Availability Statement: The data used to support the findings of this study are available from the corresponding authors upon request.

Conflicts of Interest: The authors declare that there are no conflicts of interest regarding the publication of this paper.

References

1. Yıldız, H.; Bahçeci, D.; Kızılkaya, B. Hidden engineering in molecular silence: Examination of biomineralization structure in the shell of *Magallana gigas* (Thunberg, 1793) species using X-ray diffraction (XRD). *Mar. Sci. Technol. Bull.* **2025**, *14*, 94–102. [CrossRef]
2. Nahle, S.; Lutet-Toti, C.; Namikawa, Y.; Piet, M.-H.; Brion, A.; Peyroche, S.; Suzuki, M.; Marin, F.; Rousseau, M. Organic Matrices of Calcium Carbonate Biominerals Improve Osteoblastic Mineralization. *Mar. Biotechnol.* **2024**, *26*, 539–549. [CrossRef] [PubMed]
3. Morris, J.P.; Backeljau, T.; Chapelle, G. Shells from aquaculture: A valuable waste, not a problem. *J. Rev. Aquac.* **2019**, *11*, 42–57. [CrossRef]
4. Kassim, U.; Topić Popović, N.; Lorencin, V.; Strunjak-Perović, I.; Čož-Rakovac, R. Shell Waste Management and Utilization: Mitigating Organic Pollution and Enhancing Sustainability. *Appl. Sci.* **2023**, *13*, 623. [CrossRef]
5. Su, J.; Wang, J. Preparation and performance study of shell micropowder based refractory cement. *Concrete* **2025**, *2*, 114.
6. Kassim, U. Performance of Concrete Incorporating of Clam Shell as Partially Replacement of Ordinary Portland Cement (OPC). *J. Adv. Res. Appl. Mech.* **2019**, *55*, 12–21.
7. Chen, F.; Teng, Y.; Wu, W.; Zhao, F. Research on the Impact of High Dosage Shell Powder on the Durability of Concrete. *Railw. Constr. Technol.* **2025**, *6*, 53–56,147.
8. Jeong, Y.; Hargis, C.W.; Chun, S.; Moon, J. Effect of Calcium Carbonate Fineness on Calcium Sulfoaluminate-Belite Cement. *Materials* **2017**, *10*, 900. [CrossRef]
9. Naqi, A.; Siddique, S.; Kim, H.-K.; Jang, J.G. Examining the potential of calcined oyster shell waste as additive in high volume slag cement. *Constr. Build. Mater.* **2020**, *230*, 116973. [CrossRef]
10. Ma, J.; Yu, Z.; Ni, C.; Shi, H.; Shen, X. Effects of limestone powder on the hydration and microstructure development of calcium sulphoaluminate cement under long-term curing. *Constr. Build. Mater.* **2019**, *199*, 688–695. [CrossRef]
11. Jing, Q. Influence of Oyster Shell Powder on Workability, Strengths and Shrinkage of Potassium Magnesium Phosphate Cement. *J. Munic. Technol.* **2023**, *4*, 189–193.
12. Chong, L.; Shi, C.; Yang, J.; Jia, H. Effect of limestone powder on the water stability of magnesium phosphate cement-based materials. *Constr. Build. Mater.* **2017**, *148*, 590–598. [CrossRef]
13. Yang, B.; Han, Y.; Kong, Z.; Wang, X. Effect of waste oyster shell powder on the micro- and macroproperties and sustainable performance of cement-based materials. *J. Build. Eng.* **2024**, *92*, 109800. [CrossRef]
14. Xu, M.; Wang, W.; Li, N.; Wang, Y.; Jiang, P.; Hu, J.; Xiao, L. Soil utilization of solid waste: Small strain characteristics of coastal cement soil modified by oyster shell powder under freeze-thaw cycle. *Case Stud. Constr. Mater.* **2025**, *23*, e05055. [CrossRef]
15. Liao, Y.; Fan, J.; Li, R.; Da, B.; Chen, D.; Zhang, Y. Influence of the usage of waste oyster shell powder on mechanical properties and durability of mortar. *Adv. Powder Technol.* **2022**, *33*, 103503. [CrossRef]
16. Pourchet, S.; Regnaud, L.; Perez, J.P.; Nonat, A. Early C3A hydration in the presence of different kinds of calcium sulfate. *Cem. Concr. Res.* **2009**, *39*, 989–996. [CrossRef]
17. Wang, Y.; Jia, J.; Zhang, D.; Gao, X. New Insights into the Effect of Calcium Formate on the Hydration Process of Tricalcium Silicate. *J. Mater. Civ. Eng.* **2025**, *37*, 04025033. [CrossRef]
18. De Belie, N.; Grosse, C.U.; Kurz, J.; Reinhardt, H.W. Ultrasound monitoring of the influence of different accelerating admixtures and cement types for shotcrete on setting and hardening behavior. *Cem. Concr. Res.* **2005**, *35*, 2087–2094. [CrossRef]
19. Rashad, A.; Khalil, M.; Shaltout, A. Calcium formate as a modifier agent for calcium hydroxide-activated slag cement. *J. Eng. Appl. Sci.* **2025**, *72*, 183. [CrossRef]
20. Wang, H.; Wang, A.; Wang, J.; Zhang, J.; Du, T.; Shen, J. Optimizing quaternary chemical additives and steel fiber dispersion in CSA cement based HPC for rapid repair engineering. *Constr. Build. Mater.* **2025**, *489*, 142265. [CrossRef]

21. Xing, Z.; Guo, Y.; Zhu, Y.; Chen, L. Deterioration pattern of the axial compressive properties of steel-reinforced concrete columns owing to chloride salt erosion. *Eng. Struct.* **2024**, *313*, 118169. [CrossRef]
22. Jiang, H.; Tian, D.; Dong, M.; Lv, M.; Yang, X.; Lu, S. Effects of interlayer-modified layered double hydroxides with organic corrosion inhibiting ions on the properties of cement-based materials and reinforcement corrosion in chloride environment. *Cem. Concr. Compos.* **2024**, *154*, 106793. [CrossRef]
23. Xia, Z.; Geng, J.; Zhou, Z.; Liu, G. Comparative analysis of polypropylene, basalt, and steel fibers in 3D printed concrete: Effects on flowability, printabiliy, rheology, and mechanical performance. *Constr. Build. Mater.* **2025**, *465*, 140098. [CrossRef]
24. *GB/T 27690-2023*; Silica Fume for Mortar and Concrete. State Administration for Market Regulation. Standardization Administration of the People's Republic of China: Beijing, China, 2023.
25. *GB 175-2023*; Common Portland Cement. State Administration for Market Regulation. Standardization Administration of the People's Republic of China: Beijing, China, 2023.
26. *GB/T 14684-2022*; Sand for Construction. State Administration for Market Regulation. Standardization Administration of the People's Republic of China: Beijing, China, 2022.
27. *GB 8076-2008*; Concrete Admixtures. General Administration of Quality Supervision, Inspection and Quarantine of the People's Republic of China. Standardization Administration of the People's Republic of China: Beijing, China, 2008.
28. *JGJ/T 70-2009*; Standard for Test Method of Performance on Building Mortar. Ministry of Housing and Urban-Rural Development of the People's Republic of China: Beijing, China, 2009.
29. *GB/T 2419-2005*; Test Method for Fluidity of Cement Mortar. State Administration for Market Regulation: Beijing, China, 2005.
30. *GB/T 17671-2021*; Methods for Testing Cement—Determination of Strength. State Administration for Market Regulation: Beijing, China, 2021.
31. *JC/T 603-2004*; Standard Test Method for Drying Shrinkage of Mortar. National Development and Reform Commission of the People's Republic of China: Beijing, China, 2004.
32. *GB/T 50082-2024*; Standard for Test Methods of Long-Term Performance and Durability of Concrete. Standardization Administration of the People's Republic of China: Beijing, China, 2024.
33. Bahadori, H.R.; Hedayat, A.A.; Karbakhsh, A.; Mohammadizadeh, M. Effects of Seashell and Lumashell powders on the elevated temperature compressive strength and durability of shell-based concretes. *Innov. Infrastruct. Solut.* **2023**, *8*, 199. [CrossRef]
34. Kwon, S.J.; Wang, X. A Hydration-Based Integrated Model to Evaluate Properties Development and Sustainability of Oyster Shell Powder-Cement Binary Composites. *Buildings* **2024**, *14*, 1578. [CrossRef]
35. Liao, Y.; Shi, H.; Zhang, S.; Da, B.; Chen, D. Particle Size Effect of Oyster Shell on Mortar: Experimental Investigation and Modeling. *Materials* **2021**, *14*, 6813. [CrossRef]
36. Liao, Y.; Wang, X.; Feng, W.; Meng, Y.; Chen, D.; Da, B. Influence of mineral admixtures on the mechanical property and durability of waste oyster shell mortar. *J. Southeast Univ. (Engl. Ed.)* **2023**, *39*, 277–283.
37. Ge, W.; Zhang, Z.; Ashour, A.; Li, W.; Jiang, H.; Hu, Y.; Shuai, H.; Sun, C.; Li, S.; Liu, Y. Hydration characteristics, hydration products and microstructure of reactive powder concrete. *J. Build. Eng.* **2023**, *69*, 106306. [CrossRef]
38. Cheung, J.; Roberts, L.; Patel, D. Cement hydration mechanisms through time—A review. *J. Mater. Sci.* **2023**, *58*, 9805–9833.
39. Hemalatha, T.; Arthi, K.; Mapa, M. Effect of calcium formate on hydration mechanism of cement fly ash blends. *ACI Mater. J.* **2019**, *116*, 51–59. [CrossRef]
40. Huang, T.; Yuan, Q.; Zuo, S.; Xie, Y.; Shi, C. New insights into the effect of gypsum on hydration and elasticity development of C3S paste during setting. *Cem. Concr. Res.* **2022**, *159*, 106860. [CrossRef]
41. Seifu, M.N.; Park, J.K.; Han, T.H.; Park, S.; Kim, M.O. Effect of oyster shell powder addition on hydration of Portland cement-calcium sulfoaluminate cement-blast furnace slag or -metakaolin ternary cement. *Case Stud. Constr. Mater.* **2022**, *17*, e01529. [CrossRef]
42. Hu, H.B.; Ma, X.S.; Zuo, J.Q.; She, A.M.; Wei, Y.Q.; Yao, W.; Wu, M. High-volume fly ash mortar mixes containing waste dolomite powders: Early-age properties, hydration characteristics, microstructure, and sustainability assessment. *Constr. Build. Mater.* **2025**, *484*, 141899. [CrossRef]
43. Liao, Y.D.; Wang, X.; Wang, L.; Yin, Z.X.; Da, B.; Chen, D. Effect of waste oyster shell powder content on properties of cement-metakaolin mortar. *Case Stud. Constr. Mater.* **2022**, *16*, e01088. [CrossRef]
44. Cheng, L.; Kong, D.; Huang, Y.; Wang, Y.; Liu, P.; Zhang, Y. Research on the Strength and Thermal Conductivity of Basalt Fiber Reinforced Phosphogypsum-Based Composite Cementitious Materials. *Mech. Compos. Mater.* **2025**, *436*, 136955. [CrossRef]
45. Hong, X.; Wang, H.; Shi, F. Influence of NaCl freeze thaw cycles and cyclic loading on the mechanical performance and permeability of sulphoaluminate cement reactive powder concrete. *Coatings* **2020**, *10*, 1227. [CrossRef]
46. Huang, G.; Wang, H.; Shi, F. Coupling Effect of Salt Freeze-Thaw Cycles and Carbonation on the Mechanical Performance of Quick Hardening Sulphoaluminate Cement-Based Reactive Powder Concrete with Basalt Fibers. *Coatings* **2021**, *11*, 1142. [CrossRef]
47. Shan, Z.; Yin, G.; Wen, X.; Miao, L.; Wang, S.; Zuo, X. Numerical simulation on transport-crystallization-mechanical behavior in concrete structure under external sulfate attack and wetting-drying cycles. *Mater. Des.* **2024**, *241*, 112908. [CrossRef]

48. Agunsoye, J.; Madueke, C.; Bamigbaiye, A.; Agbakansi, K.; Oladipo, A. The Development and Characterisation of Recycled Polyethylene Reinforced Particulate Cockle Shell for Automobile Application. *J. Eng. Technol.* **2021**, *6*, 92–95. [CrossRef]
49. Georges, M.; Bourguiba, A.; Chateigner, D.; Sebaibi, N.; Boutouil, M. The study of long-term durability and bio-colonization of concrete in marine environment. *Environ. Sustain. Indic.* **2021**, *10*, 100120. [CrossRef]
50. Lu, L.; Dong, O. Properties of Cement Mortar and Ultra-High Strength Concrete Incorporating Graphene Oxide Nanosheets. *Nanomaterials* **2017**, *7*, 187. [CrossRef] [PubMed]
51. Wu, Z.; Shi, C.; He, W.; Wu, L. Effects of steel fiber content and shape on mechanical properties of ultra high performance concrete. *Constr. Build. Mater.* **2016**, *103*, 8–14. [CrossRef]
52. Yang, H. Influence of Mineral Powder and Fiber on Work and Mechanical Properties of Reactive Powder Concrete. *Multipurp. Util. Miner. Resour.* **2023**, *2*, 197–204.

Disclaimer/Publisher's Note: The statements, opinions and data contained in all publications are solely those of the individual author(s) and contributor(s) and not of MDPI and/or the editor(s). MDPI and/or the editor(s) disclaim responsibility for any injury to people or property resulting from any ideas, methods, instructions or products referred to in the content.